OPEN

IDEAS AND INNOVATIONS
PEDIATRIC/CRANIOFACIAL

Topological Analysis for Arteriovenous Malformations via Computed Tomography Angiography: Part 1: Mathematical Concepts

Yuki Hata, MD*
Keigo Osuga, MD, PhD†
Tateki Kubo, MD, PhD*
Ken Matsuda, MD, PhD*
Koichi Tomita, MD, PhD*
Mamoru Kikuchi, MD, PhD*
Takashi Fujiwara, MD*
Kenji Yano, MD, PhD*
Ko Hosokawa, MD, PhD*

Background: Evaluating the progression of soft-tissue arteriovenous malformation (AVMs) is still problematic. To establish a quantitative method, we took a morphological approach.
Methods: Normal blood vessels in early-phase 3D-computed tomography angiography images are theoretically expected to be tree-like structures without loops, whereas AVM blood vessels are expected to be mesh-like structures with loops. Simplified to the utmost limit, these vascular structures can be symbolized with wire-frame models composed of nodes and connecting edges, in which making an extra loop always needs one more of edges than of nodes.
Results: Total amount of abnormal vascular structures is estimated from a simple equation: Number of vascular loops = 1 − ([Number of nodes] − [Number of edges]).
Conclusion: Abnormalities of AVM vascular structures can be mathematically quantified using computed tomography angiography images. *(Plast Reconstr Surg Glob Open 2014;2:e205; doi: 10.1097/GOX.0000000000000163; Published online 28 August 2014.)*

Soft-tissue arteriovenous malformations (AVMs) progress asymptomatically or recur indistinguishably from normal blood vessels. Despite that, understanding of their progression usually relies on approximate staging according to symptoms[1] or qualitative visual assessment of imaging examinations. Against this dilemma, numerous attempts have been made to establish quantitative evaluation methods.

*From the *Department of Plastic Surgery, Osaka University Graduate School of Medicine, Osaka, Japan; and †Department of Diagnostic and Interventional Radiology, Osaka University Graduate School of Medicine, Osaka, Japan.*
Received for publication December 27, 2013; accepted June 25, 2014.

DOI: 10.1097/GOX.0000000000000163

From a functional viewpoint, evaluation of total shunt blood flow using transarterial lung perfusion scans[2–4] and measurement of blood pool volume with whole-body blood pool scans by Lee et al[2,4,5] are the most quantitative methods. However, these methods based on nuclear medicine are problematic for their invasion and limited site of application.

From a morphometric viewpoint, Kaji et al[6] used magnetic resonance imaging and World Health Organization Response Criteria (product of lesion major and minor axes in cross-section). However, it is difficult to apply it to vascular malformations, which are irregular in shape with indistinct borders, easily expanding and collapsing.

Considering these unmet needs, we searched for another approach to meet the anatomical nature of AVMs and set the first research objective to establish a morphological solution to quantify abnormalities of AVM vascular structures.

Disclosure: *The authors have no financial interest to declare in relation to the content of this article. The Article Processing Charge was paid for by the authors.*

METHODS

We anticipated utilization of computed tomography angiography (CTA) results for retrospective evaluation because it is a widespread, less-invasive method of testing AVMs. Moreover, because of their relatively higher contrast, obtaining clear and stable vascular segmentation[7] is easier than Magnetic Resonance Angiography (MRA).[8–10]

We also applied 2 mathematical theories, namely topology and graph theory, to quantify abnormalities of vascular structures.

Simplification via Topological Homeomorphism

Topology is a relatively new field of geometry that focuses on the continuity of regions. For example, as both a coffee cup and a donut share the feature of having only one hole (loop), they are considered homeomorphic with deformation.

Viewed through homeomorphic simplification, the number of loops in an early-phase 3D-CTA image of a normal blood vessel is theoretically expected to be close to zero except for physiological vascular rings, such as at the base of the brain. It is because arteries branch off repeatedly from the aorta and are not rendered with the standard CT resolution after they become arterioles (approximate diameter, 0.1–0.2 mm) (Fig. 1).

Meanwhile, the presence of a described arteriovenous shunt is depicted on early-phase 3D-CTA images as a series of pathways from the feeding artery to the drainage vein. Furthermore, the more abnormal intervascular shortcut appears, the more external loop develops or an existing loop divides.

Quantification of Connectivity with Graph Theory

The appropriate method for loop measurement is graph theory, which is being utilized for engineering problems such as electric circuits and train routes.

If one focuses only on connectivity and dispenses with all other data such as thickness and length, the vascular structure can ultimately be symbolized into a "graph" composed of nodes and edges joining them. The number of loops in the graph can be calculated by a simple calculation using the number of nodes and edges. The principle can be verified and understood by using our "spaghetti and marshmallows vascular model." This model can be actually manipulated according to only one rule that a marshmallow (node) must be positioned on the tip of each piece of spaghetti (edge).

When a model only diverges and expands repeatedly like the branches or roots of a tree, the total number of nodes keeps one more than edges. It is because one node is needed for every new edge when branches are added or divided (Fig. 2A).

However, when nodes and edges are added to increase the number of loops, the number of edges will only increase by one extra piece each time. This is because even if a new loop is added or the existing loop is divided, one more edge is needed compared with nodes (Fig. 2B).

RESULTS

Aforementioned mathematical concepts lead to a principle that abnormal connectivities within an AVM lesion can be quantified with the increase of difference between the number of nodes and edges comprising its wire-framed network model. This principle is depicted by the following simple equation:

$$\text{Number of vascular loops} = 1 - (\text{[Number of nodes]} - \text{[Number of edges]}).$$

DISCUSSION

Fundamental Limitation

In clinical applications, there is an inevitable limitation that the number of vascular loops calculated from CTA images is not necessarily the histological amount of arteriovenous shunts within the actual lesion but "describable" shunts to the utmost. However, it is rather the common fundamental limitation for all imaging examinations.

Resolution Constancy

There are 2 important points regarding this technique. The first is that image resolution affects the detection of continuity. For example, the relationship of a blood vessel with its accompanying vessel 0.3 mm away can be sometimes correctly displayed on an image with 0.27 × 0.27 mm pixel size but invari-

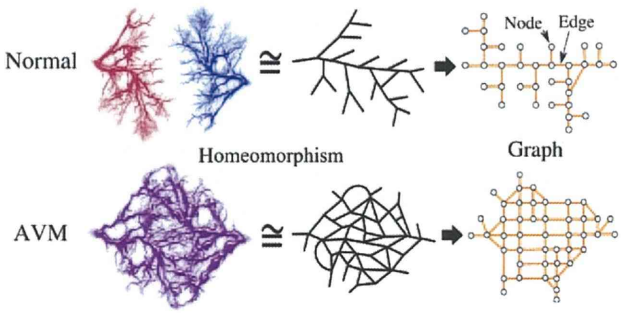

Fig. 1. Conceptual workflow images of homeomorphic simplification and symbolization of vascular structures. AVM graphs are assumed to be more perforated than normal blood vessel graphs.

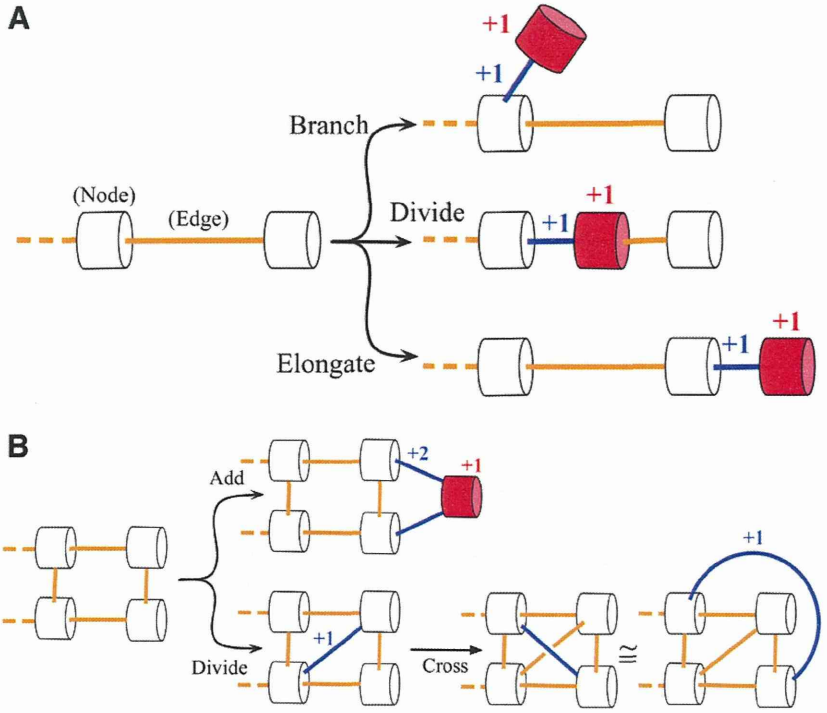

Fig. 2. Verification of graph theory with "spaghetti and marshmallows vascular models." A, Tree-type growth: when a model only diverges and expands repeatedly like the branches or roots of a tree, the gap of nodes and edges never changes. B, Mesh-type growth: when nodes and edges are added to increase the number of loops from that of the original model, the number of edges will only increase by one extra piece each time. This principle holds true even in 3-dimensionally (3D) complex angioarchitecture because an internal 3D crossing is topologically homeomorphic with an external handle.

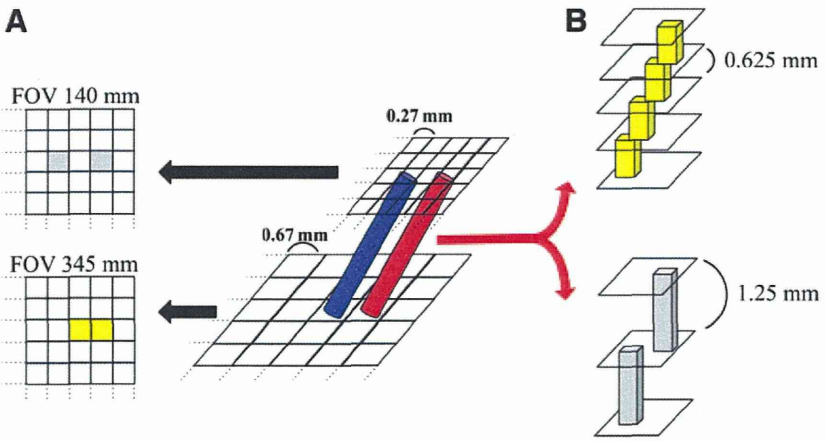

Fig. 3. The influence of imaging conditions. A, When a computed tomography section is provided as a 512×512 pixel image, the relationship of a blood vessel with its accompanying vessel 0.3 mm away can be sometimes correctly displayed on a 140-mm field-of-view (FOV) (pixel size, 0.27×0.27 mm) image of the peripheral extremities, while the same 2 vessels can invariably be displayed as being connected on a 345-mm FOV (pixel size, 0.67×0.67 mm) image of the trunk. B, Vessels rendered as continuous on images with a section thickness of 0.625 mm might appear to be not continuous on images with section thicknesses of 1.25 mm.

ably be displayed as being connected on an image with 0.67 × 0.67 mm pixel size (Fig. 3A).

Conversely, oblique vessels rendered as continuous on images with a section thickness of 0.625 mm might appear to be not continuous on images with section thicknesses of 1.25 mm (Fig. 3B).

Field of view and section thickness must be identical to compare test results obtained at different times from a same patient. In addition, even in patients with a common lesion site, the closer the test field of view and section thickness are, the more meaningful the comparison is.

Region of Interest Constancy

The second point is that one cannot be sure that region of interest has been uniformly maintained through the series of results especially when efficient procedure causes drastic change to the lesion hemodynamics. Region of interest must be identical before and after treatment, which is possible if clear, fixed points such as the junctions of well-known blood vessels or feeding arteries are used as reference points.

CONCLUSIONS

It seems that the mathematical concepts of topology and graph theory can be used to quantify abnormalities of AVM vascular structures from CTA images. Careful assessment of validity through practical application is necessary for this novel concept.[11]

Yuki Hata, MD
Department of Plastic Surgery
Osaka University Graduate
School of Medicine, Osaka, Japan
E-mail: yukihata@gmail.com

REFERENCES

1. Kohout MP, Hansen M, Pribaz JJ, et al. Arteriovenous malformations of the head and neck: natural history and management. *Plast Reconstr Surg.* 1998;102:643–654.
2. Lee BB, Do YS, Yakes W, et al. Management of arteriovenous malformations: a multidisciplinary approach. *J Vasc Surg.* 2004;39:590–600.
3. Vaišnytė B, Vajauskas D, Palionis D, et al. Diagnostic methods, treatment modalities, and follow-up of extracranial arteriovenous malformations. *Medicina (Kaunas).* 2012;48:388–398.
4. Lee BB, Mattassi R, Kim YW, et al. Advanced management of arteriovenous shunting malformation with transarterial lung perfusion scintigraphy for follow-up assessment. *Int Angiol.* 2005;24:173–184.
5. Lee BB, Mattassi R, Kim BT, et al. Contemporary diagnosis and management of venous and arterio-venous shunting malformation by whole body blood pool scintigraphy. *Int Angiol.* 2004;23:355–367.
6. Kaji N, Kurita M, Ozaki M, et al. Experience of sclerotherapy and embolosclerotherapy using ethanolamine oleate for vascular malformations of the head and neck. *Scand J Plast Reconstr Surg Hand Surg.* 2009;43:126–136.
7. Moore EA, Grieve JP, Jäger HR. Robust processing of intracranial CT angiograms for 3D volume rendering. *Eur Radiol.* 2001;11:137–141.
8. Suazo L, Foerster B, Fermin R, et al. Measurement of blood flow in arteriovenous malformations before and after embolization using arterial spin labeling. *Interv Neuroradiol.* 2012;18:42–48.
9. Albert CS, Chung JAN. Statistical 3d vessel segmentation using a rician distribution. Available at: http://citeseerx.ist.psu.edu/viewdoc/summary?doi=10.1.1.75.2885. Accessed June 27, 2013.
10. Bullitt E, Aylward S, Bernard EJ, et al. Computer-assisted visualization of arteriovenous malformations on the home personal computer. *Neurosurgery* 2001;48:576–582; discussion 582–583.
11. Hata Y, Osuga K, Uehara S, et al. Topological analysis for arteriovenous malformations via computed tomography angiography: part 2: practical application. *Plast Reconstr Surg Glob Open* 2014. doi: 10.1097/GOX.0000000000000151.

Tanigawa et al. BMC Complementary and Alternative Medicine 2014, 14:133
http://www.biomedcentral.com/1472-6882/14/133

BMC
Complementary & Alternative Medicine

RESEARCH ARTICLE Open Access

(+)-Catechin protects dermal fibroblasts against oxidative stress-induced apoptosis

Tomoko Tanigawa[1], Shigeyuki Kanazawa[1*], Ryoko Ichibori[1], Takashi Fujiwara[1], Takuya Magome[2], Kenta Shingaki[3], Shingo Miyata[4], Yuki Hata[1], Koichi Tomita[1], Ken Matsuda[5], Tateki Kubo[1], Masaya Tohyama[3], Kenji Yano[1] and Ko Hosokawa[1]

Abstract

Background: Oxidative stress has been suggested as a mechanism underlying skin aging, as it triggers apoptosis in various cell types, including fibroblasts, which play important roles in the preservation of healthy, youthful skin. Catechins, which are antioxidants contained in green tea, exert various actions such as anti-inflammatory, anti-bacterial, and anti-cancer actions. In this study, we investigated the effect of (+)-catechin on apoptosis induced by oxidative stress in fibroblasts.

Methods: Fibroblasts (NIH3T3) under oxidative stress induced by hydrogen peroxide (0.1 mM) were treated with either vehicle or (+)-catechin (0–100 μM). The effect of (+)-catechin on cell viability, apoptosis, phosphorylation of c-Jun terminal kinases (JNK) and p38, and activation of caspase-3 in fibroblasts under oxidative stress were evaluated.

Results: Hydrogen peroxide induced apoptotic cell death in fibroblasts, accompanied by induction of phosphorylation of JNK and p38 and activation of caspase-3. Pretreatment of the fibroblasts with (+)-catechin inhibited hydrogen peroxide-induced apoptosis and reduced phosphorylation of JNK and p38 and activation of caspase-3.

Conclusion: (+)-Catechin protects against oxidative stress-induced cell death in fibroblasts, possibly by inhibiting phosphorylation of p38 and JNK. These results suggest that (+)-catechin has potential as a therapeutic agent for the prevention of skin aging.

Keywords: Catechin, Fibroblast, Apoptosis, Oxidative stress

Background

Skin wrinkles and sagging are important factors defining skin youthfulness. Development of methods to reduce skin wrinkles and prevent sagging skin has become an important research topic in aesthetic and anti-aging medicine. Skin wrinkles and sagging are reported to be influenced by the amount of collagen, elastin, and hyaluronic acid [1]. Fibroblasts play a key role in the production of these extracellular matrix components in the skin. Skin aging is the consequence of reduced numbers of fibroblasts, lower levels of extracellular matrix proteins, and decreased skin elasticity and tonus, thereby resulting in the formation of wrinkles [2]. Therefore, maintaining the population of dermal fibroblasts is important for both preventing and treating age-related skin changes.

Oxidative stress has been indicated in a variety of pathological processes, such as atherosclerosis, diabetes, neurodegenerative diseases, and aging. Reactive oxygen species induce DNA damage, intracellular lipid peroxidation, and abnormal protein oxidation reactions, all of which result in cell damage. Oxidative stress also promotes skin aging [3]; it reduces the number of skin fibroblasts by inducing apoptosis and decreasing their regenerative capacity, which in turn leads to increased skin sagging. Therefore, suppression of oxidative stress-induced apoptosis in skin fibroblasts is a potential treatment and prevention strategy for maintaining healthy youthful skin.

Green tea, which is routinely consumed in Japan and China, is widely known as a healthy drink containing various antioxidants, vitamins, and minerals. Catechins, including (−)-epigallocatechin gallate (EGCG), (−)-epigallocatechin

* Correspondence: kanazawa@psurg.med.osaka-u.ac.jp
[1]Department of Plastic Surgery, Osaka University Graduate School of Medicine, Suita-shi, Osaka, Japan
Full list of author information is available at the end of the article

(EGC), (−)-epicatechin gallate (ECG), and (−)-epicatechin (EC) (Figure 1), account for approximately 10% of the dry weight of green tea leaves. Catechins are thought to not only possess antioxidant effects to control active oxygen [4-7] but also exert various actions, such as anti-inflammatory [8], antibacterial [9,10], and anti-cancer [11-13] actions.

In this study, we demonstrate that (+)-catechin has an inhibitory effect against oxidative stress-induced apoptosis in fibroblasts, accompanied by suppression of phosphorylation of p38 and c-Jun terminal kinases (JNK), both of which play an important role in intracellular apoptotic signaling induced by oxidative stress.

Methods

Cell culture

NIH 3T3 fibroblasts were used for all experiments. Cells were cultured in Dulbecco's Modified Eagle Medium (DMEM; Life Technologies CA, USA) containing 10% fetal bovine serum (FBS), 100 U/ml penicillin, and 100 μg/ml streptomycin (Life Technologies) in a humidified incubator at 37°C with 5% CO_2. All experiments were performed in triplicate.

Cell viability assay

Cell survival was determined using the 3-(4,5-dimethylthiazole-2-yl)-2,5-diphenyltetrazolium bromide (MTT) assay (CellTiter 96® AQueous One Solution Cell Proliferation Assay; Promega, WI, USA). Fibroblasts were plated at a density of 5,000 cells per well on 96-well plates and incubated for 24 h in 100 μl of DMEM containing 10% FBS. After incubation with serum-free medium for 24 h, cells were treated for 30 min with various concentrations of (+)-catechin (0–400 μM; Sigma Aldrich, PA, USA), and then subjected to oxidative stress induction with 0.1 mM hydrogen peroxide (H_2O_2). After 24 h, 20 μl of One Solution Reagent was added into each well and incubated at 37°C for 2 h in a humidified, 5% CO_2 atmosphere. The production of formazan by viable cells was detected by measuring the absorbance at 490 nm using a 96-well plate reader.

Another series of experiments were conducted to compare cytotoxicity between (+)-catechin and EGCG. Fibroblasts were treated with various concentrations of (+)-catechin or EGCG (0–400 μM; Sigma Aldrich) without H_2O_2 for 24 h and the cells were then subjected to MTT assay.

TUNEL staining

Apoptosis was determined by terminal deoxynucleotidyl transferase (TdT)-mediated dUTP-biotin nick end labeling (TUNEL) using the *In Situ* Cell Death Detection Kit TMR Red (Roche, Mannheim, Germany), according to

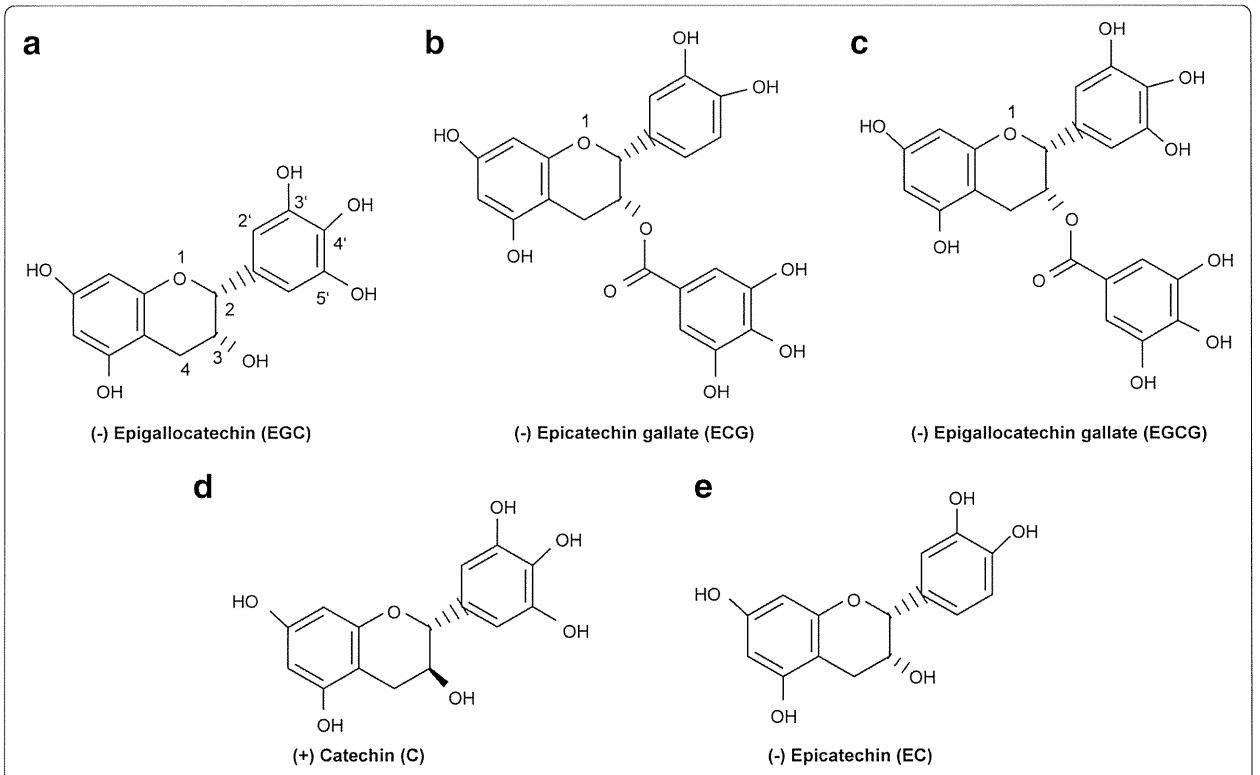

Figure 1 Chemical Structures of catechins. Structures of (−)-epigallocatechin (EGC) **(a)**, (−)-epicatechin gallate (ECG) **(b)**, (−)-epigallocatechin gallate (EGCG) **(c)**, (+)-catechin(C) **(d)**, and (−)-epicatechin (EC) **(e)**.

the manufacturer's instructions. In brief, fibroblasts were maintained in DMEM containing 10% FBS for 2 days and then cultured in serum-free DMEM. Oxidative stress was induced by addition of 0.1 mM H_2O_2 prior to treatment with 10 μM (+)-catechin or vehicle. After 24 h of incubation with H_2O_2 and (+)-catechin or vehicle, cells were fixed with 4% paraformaldehyde in phosphate-buffered saline (PBS) (pH 7.4) for 60 min at room temperature, followed by five washes with PBS. Next, permeabilization was performed by incubation with 0.1% Triton X-100 in PBS for 10 min, and cells were mixed with TUNEL reaction mixtures containing TdT and tetramethylrhodamine (TMR) red-labeled nucleotides for 1 h. Coverslips were mounted onto slides using VECTASHIELD Mounting Medium with 4′,6-diamidino-2-phenylindole dihydrochloride (Vector Laboratories, Peterborough, England). Fluorescence images were taken using a microscope (IX-70; Olympus) equipped with a charge-coupled device camera (CoolSNAP HQ; Nippon Roper, Chiba, Japan). For each experiment, 100 cells were randomly selected, and the percentage of TUNEL-positive cells was measured.

Western blot analysis

Cultured fibroblasts were serum-starved for 24 h in serum-free DMEM and then incubated with 10 μM (+)-catechin for 30 min prior to oxidative stress induction by 0.1 mM H_2O_2. After H_2O_2 challenge for 1 h, cells were harvested and lysed in radioimmunoprecipitation assay buffer containing 1 mM Na_3VO_4, 1 mM NaF, and Protease Inhibitor Cocktail (Roche Diagnostics, Basel, Switzerland) for 20 min at 4°C. After centrifugation at 15,000 × *g* for 15 min at 4°C, proteins were separated by sodium dodecyl sulfate-polyacrylamide gel electrophoresis and transferred onto Immobilon-P Transfer Membranes (Millipore Japan, Tokyo, Japan). Membranes were incubated for 60 min in Tris-buffered saline containing 5% skim milk and 0.05% Tween-20 and then blotted with the following primary antibodies at 4°C overnight: anti-phospho-JNK (1:1,000), anti-JNK (1:1,000), anti-phospho-p38 (1:1,000), anti-p38 (1:1,000), anti-cleaved caspase-3 (1:200), and anti-caspase-3 antibodies (1:200). All antibodies were purchased from Cell Signaling Technology, MA, USA. Next, membranes were incubated for 1 h with an anti-mouse or anti-rabbit HRP-linked secondary antibody (1:2,000; Cell Signaling Technology). Reaction products were visualized by chemiluminescence detection using the ECL Western Blotting Detection System (GE Healthcare, Piscataway, NJ, USA). Quantification of relative band densities was performed by densitometry using Image J software (National Institutes of Health, Bethesda, MD, USA).

Statistical analysis

All data shown are expressed as the mean ± SE of three independent experiments. Data from each experiment were normalized to the respective control sample. Differences between conditions were analyzed by Student's *t* test. Multiple-group comparisons were performed using a one-way analysis of variance, followed by Tukey's post hoc test. $P < 0.05$ was considered statistically significant.

Results

Catechin increases the viability of fibroblasts

Oxidative stress is known to promote fibroblast cell death [14]. To analyze the effect of (+)-catechin on the viability of fibroblasts in response to oxidative stress, cells cultured with various concentrations (0–100 μM) of catechin were subjected to oxidative stress induction by 0.1 mM H_2O_2. The cell numbers were analyzed after 24 h. Microscopic observation and MTT assay showed that H_2O_2 induced-oxidative stress reduced cell viability, whereas (+)-catechin suppressed the effect of H_2O_2-induced oxidative stress on cell viability in a concentration-dependent manner (Figure 2a-c).

As shown in Figure 3, microscopic evaluation of the morphological changes showed that H_2O_2 supplementation in the culture media induced apoptotic cell death characterized by shrinkage of the cell body, whereas treatment with (+)-catechin attenuated H_2O_2-induced cell death.

(+)-Catechin inhibits oxidative stress-induced apoptosis in fibroblasts

To determine whether (+)-catechin has an inhibitory effect on oxidative stress-induced apoptosis in fibroblasts, we assessed the apoptosis of fibroblasts in either the presence or absence of (+)-catechin by TUNEL staining. (+)-Catechin (10 μM)-treated fibroblasts showed significant decreases in the percentage of cells positive for TUNEL staining, compared to vehicle-treated cells (9.14% ± 0.6% vs. 1.86% ± 0.3%; Figure 4).

Effect of catechin on the activation of caspase-3 by H_2O_2-induced oxidative stress in fibroblasts

Western blotting analysis using an anti-cleaved caspase-3 antibody showed that the level of cleaved caspase-3 induced by H_2O_2 was reduced by treatment with 10 μM (+)-catechin (Figure 5). These results suggest that (+)-catechin inhibits caspase-3-dependent apoptosis induced by oxidative stress in fibroblasts.

(+)-Catechin inhibits phosphorylation of p38 and JNK induced by oxidative stress

To further investigate the underlying mechanism by which (+)-catechin inhibits oxidative stress-induced apoptosis in fibroblasts, we determined whether oxidative stress-induced phosphorylation of JNK and p38 was inhibited by treatment with 10 μM (+)-catechin. The results clearly show that H_2O_2-induced phosphorylation of p38 and JNK was suppressed by (+)-catechin treatment (Figure 6).

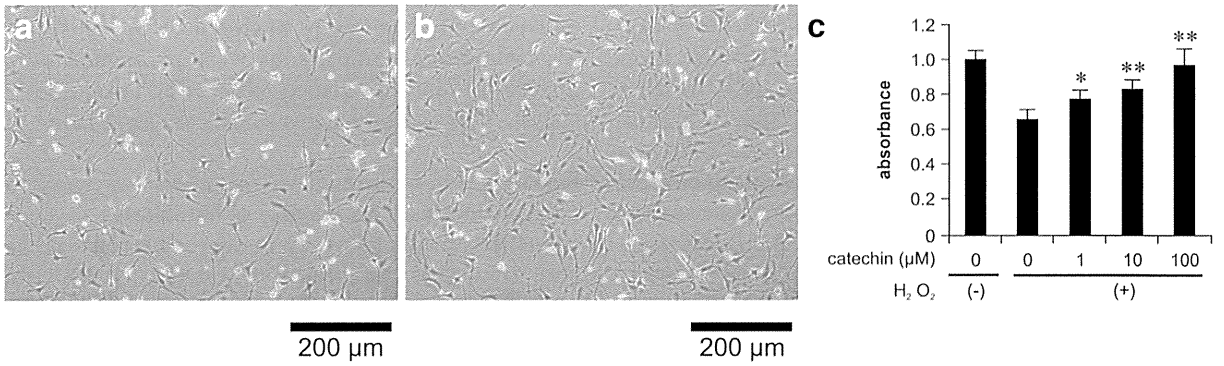

Figure 2 Inhibitory effect of (+)-catechin on oxidative stress-induced cell death in fibroblasts. After incubation with serum-free medium for 24 h, fibroblasts were treated for 30 min with (+)-catechin (0–400 μM) and then subjected to oxidative stress induction with 0.1 mM hydrogen peroxide (H_2O_2). After 24 h, cell viability was evaluated. **(a)** Representative microscopic images of cell death induced by oxidative stress **(a)** and inhibitory effect of (+)-catechin on oxidative stress-induced cell death **(b)**. Cell viability was assessed by the MTT assay **(c)**. Data are expressed as the mean ± SEM. *P < 0.05, **P < 0.01.

(+)-catechin is less cytotoxic than EGCG in fibroblasts

The MTT assay showed that fibroblasts were viable when incubated with high concentrations of (+)-catechin. In contrast, EGCG at 200 and 400 μM significantly decreased cell viability (Figure 7).

Discussion

In the present study, we demonstrate an inhibitory effect of (+)-catechin on oxidative stress-induced apoptosis in fibroblasts, accompanied by amelioration of the phosphorylation of p38 and JNK induced by oxidative stress.

We focused on fibroblasts because they participate in skin maintenance and renewal. In the skin, fibroblasts play a key role in the production of extracellular matrix components, including collagen, elastin, and hyaluronic acid. In clinical aesthetic medicine, epidermal or intradermal injection of hyaluronic acid is performed to obtain glossy and healthy skin (microinjections of hyaluronic acid, vitamins, minerals, and amino acids into the superficial layer of the skin) [15]. Other techniques, such as implanting activated fibroblasts in the skin, are also known to revive the skin to be glossy and healthy (intradermal injection of cultivated skin fibroblasts into wrinkles) [16-18]. However, these therapies are associated with a high cost and may provoke adverse events, including misplacement, allergy, nodules, necrosis, abscesses, and rejection. In contrast, the use of health supplements, such as green tea and food-derived active substances, is a safer and beneficial anti-aging method.

The integrity and functions of the skin barrier may be impaired by excessive exposure to allergens, chemicals, ultraviolet light, and dehydration. Failure of the skin barrier would subsequently lead to infections with pathogens and result in inflammatory responses. Locally produced reactive oxygen species are also known to inhibit the growth of epithelial cells and fibroblasts by inducing apoptosis and inhibiting collagen and hyaluronic acid production, all of which have been implicated in aging processes leading to skin wrinkles and sagging. Our present study suggests that (+)-catechin is a potential candidate for suppressing oxidative stress-induced apoptosis of skin fibroblasts, which may in turn reverse the reduction of fibroblast-derived

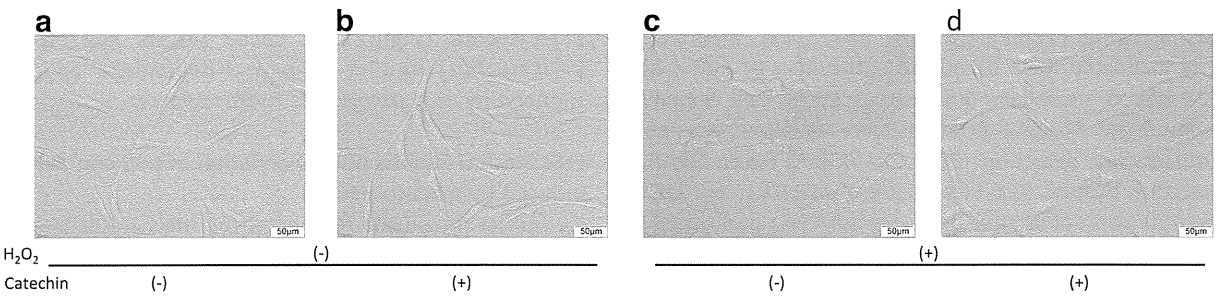

Figure 3 Microscopic images of H_2O_2-induced apoptotic cell death and inhibitory effect of (+)-catechin against H_2O_2-induced cell death. (a) The image of non-loading control cells. After incubation with serum-free medium for 24 h, fibroblasts were treated for 30 min with 10 μM (+)-catechin **(b)**, **(d)**. And then subjected to oxidative stress induction with 0.1 mM H_2O_2 **(c)**, **(d)**. After 24 h, microscopic morphological changes were evaluated.

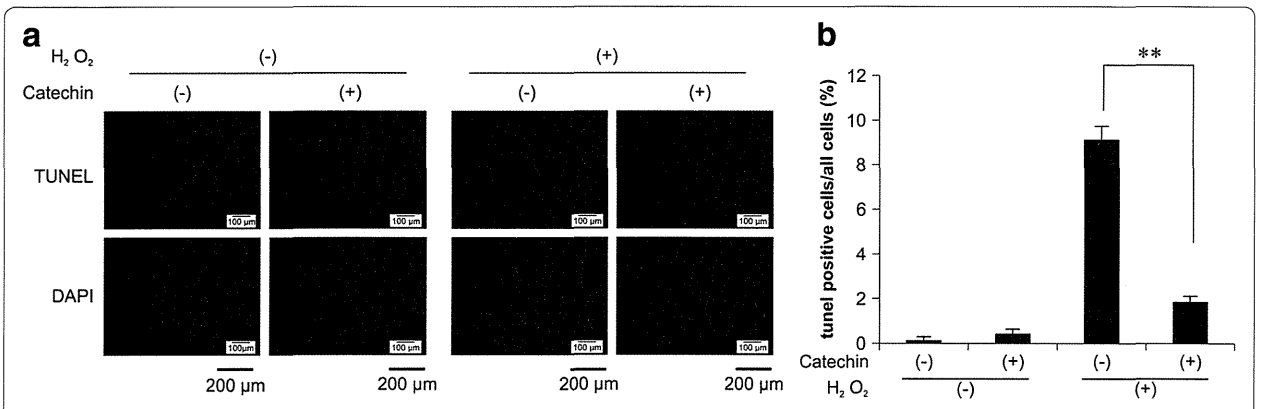

Figure 4 Inhibitory effect of (+)-catechin on oxidative stress-induced apoptosis in fibroblasts. After incubation with serum-free medium for 24 h, fibroblasts were treated for 30 min with 10 μM (+)-catechin and then subjected to oxidative stress induction with 0.1 mM hydrogen peroxide (H_2O_2). After 24 h, apoptosis was evaluated by TUNEL staining. **(a)** Microscopic findings of TUNEL staining for detection of apoptotic cells. **(b)** For evaluation of apoptosis, 100 cells were randomly selected and the percentage of TUNEL-positive cells was measured. Data are expressed as the mean ± SEM. **P < 0.01.

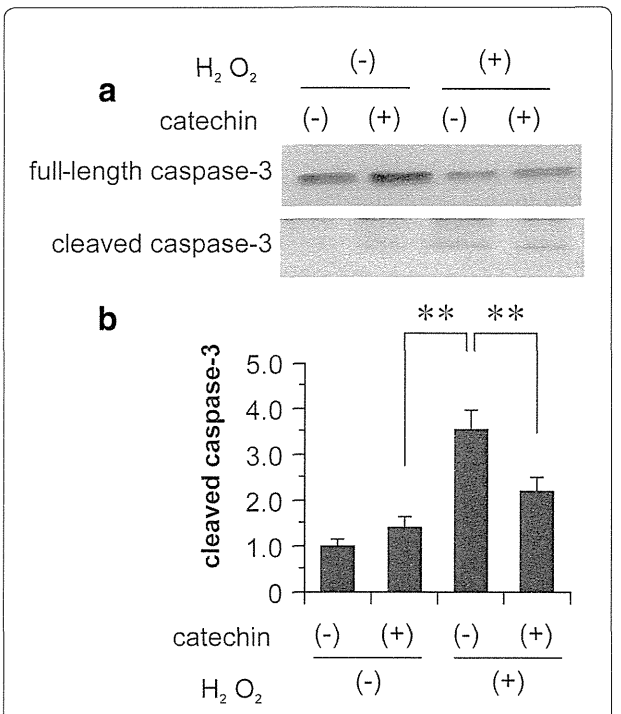

Figure 5 Effect of (+)-catechin on activation of caspase-3 by H_2O_2-induced oxidative stress in fibroblasts. After incubation with serum-free medium for 24 h, fibroblasts were treated for 30 min with 10 μM (+)-catechin and then subjected to oxidative stress induction with 0.1 mM hydrogen peroxide (H_2O_2). After 1 h, activation of caspase-3 was determined by SDS-PAGE and western blotting analysis using an anti-cleaved caspase-3 antibody. **(a)** Representative images of western blot analysis for cleaved and total caspase-3. **(b)** Expression levels of cleaved caspase-3 were normalized to those of total caspase-3. Data are expressed as the mean ± SEM. **P < 0.01.

production of collagen and hyaluronic acid. Other reports suggest that EGCG, another type of catechin, is also a potential candidate for suppressing oxidative stress-induced apoptosis of skin fibroblasts [19]; however, our present study showed that (+)-catechin is less cytotoxic than EGCG, suggesting that for therapeutic and preventive purposes (+)-catechin may be superior to EGCG.

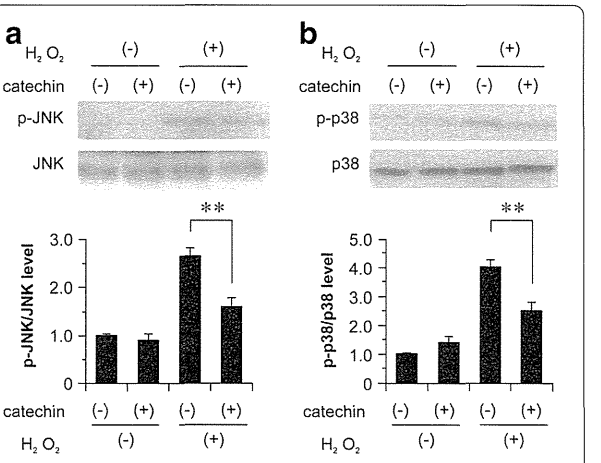

Figure 6 Inhibitory effect of (+)-catechin on phosphorylation of p38 and JNK induced by oxidative stress in fibroblasts. After incubation with serum-free medium for 24 h, fibroblasts were treated for 30 min with 10 μM (+)-catechin and then subjected to oxidative stress induction with 0.1 mM hydrogen peroxide (H_2O_2). After 1 h, cells were collected, and phosphorylation of p38 and JNK was determined by SDS-PAGE and western blotting analysis using anti-phospho p38 and anti-phospho JNK antibodies. **(a)** Results of western blotting for phosphorylation of **(a)** p38 and **(b)** JNK. Phosphorylation levels of p38 and JNK were normalized to those of total p38 and JNK, respectively. Data are expressed as the mean ± SEM. **P < 0.01.

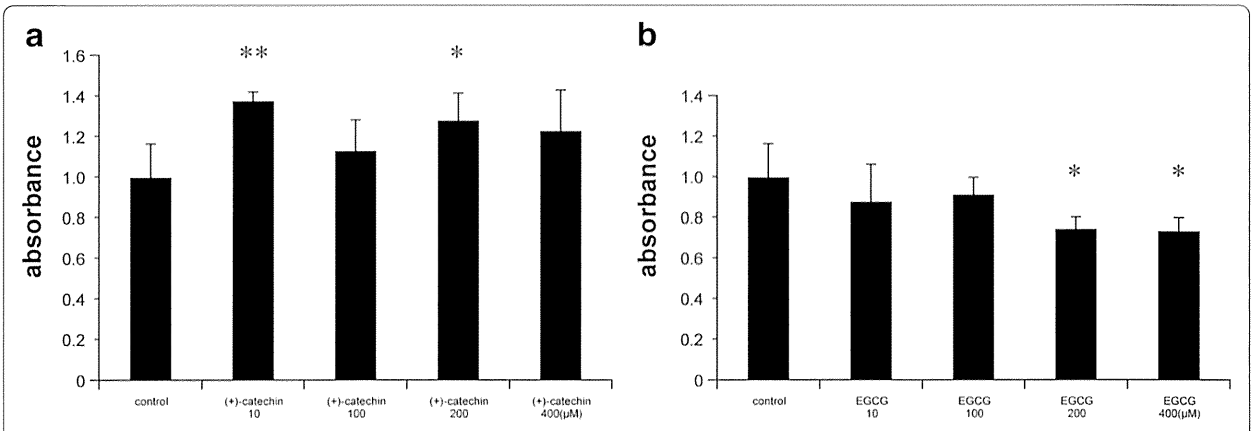

Figure 7 Comparative evaluation of cytotoxicity between (+)-catechin and EGCG in fibroblasts. Fibroblasts were treated with PBS (control) or the indicated concentrations of **(a)** (+)-catechin and **(b)** EGCG for 24 h. Cell viability was assessed by the MTT assay. Data are expressed as the mean ± SEM. *P < 0.05 and **P < 0.01.

To elucidate the underlying mechanisms by which (+)-catechin inhibits oxidative stress-induced apoptosis in fibroblasts, we focused on the effects of (+)-catechin on the phosphorylation of p38 and JNK, both of which are key molecules for oxidative stress-induced apoptosis [14]. JNK and p38 belong to the family of stress kinases and have been shown to be required for biological stress responses, such as apoptosis induced by UV, radiation, oxidative stress, heat shock, and tumor necrosis factor (TNF)-α stimulation. It has been reported that H_2O_2 signaling through TNF receptor 1 selectively activates JNK and p38 [20,21]. JNK plays an important role in controlling cell death and is known to affect the function of Bcl-2 family molecules, which suppress apoptosis. Specifically, phosphorylation of Bcl-2 by JNK results in the inhibition of Bcl-2 function and therefore induces the activation of apoptosis [20,21]. In contrast, p38 MAPK is known to be involved in the activation of apoptosis-modulating proteins, such as Fas and Bax [21]. Collectively, our present study suggests that (+)-catechin exerts anti-apoptotic effects against oxidative stress by inhibiting the phosphorylation of p38 and JNK. The precise mechanisms by which (+)-catechin suppresses the phosphorylation of JNK and p38 will be a future research topic.

Although (+)-catechin was found to exert anti-apoptotic effects in the present study, previous reports have shown both pro-apoptotic and anti-apoptotic effects of catechins. In particular, EGCG, a molecule in the same catechin group, was suggested to play a role in growth inhibition and apoptosis induction in a variety of cancer cells [22]. In contrast, EGCG was reported to have an anti-apoptotic effect in renal mesangial cells [23] and endothelial cells [24], similar to our results in the present study. Therefore, we speculate that the effect of catechins on apoptosis may vary according to cell type and the nature of pathogenesis. Given the different cell-specific responses of catechins, it is important to establish an appropriate strategy for using catechins for treatment and prevention of various diseases. It would be ideal for catechins have suppressive actions against cancers and protective effects for organs such as the kidneys and cardiovascular system. Accumulating evidence on the preventive effect of catechins and green tea against various systemic diseases, including cancers, diabetes, and hypertension, suggests little potential harm to human health from high consumption of catechins and green tea for maintenance of skin beauty.

Conclusions

(+)-Catechin exerts preventive effects against oxidative stress-induced apoptosis in fibroblasts. The underlying mechanism may involve the inhibition of p38 and JNK phosphorylation. As a safe green tea-derived antioxidant, (+)-catechin could be suitable for long-term prevention of oxidative stress-induced skin aging, considering the action of skin fibroblasts on the preservation of healthy, youthful skin.

Abbreviations

EGCG: (−)-epigallocatechin gallate; EGC: (−)-epigallocatechin; ECG: (−)-epicatechin gallate; EC: (−)-epicatechin; JNK: c-Jun terminal kinase MTT, 3-(4,5-dimethylthiazole-2-yl)-2,5-diphenyltetrazolium bromide; TdT: Terminal deoxynucleotidyl transferase; TMR: Tetramethylrhodamine; TUNEL: Terminal deoxynucleotidyl transferase (TdT)-mediated dUTP-biotin nick end labeling.

Competing interests

The authors declare that they have no competing interests.

Authors' contributions

TT designed and performed the study and wrote the manuscript. SK designed and performed the study and revised the manuscript. RY, TF, TK, KY, and KH helped to perform the study. TM, YH, KT, KM, KS, SM, and MT provided technical support. All authors read and approved the final manuscript.

Acknowledgements

This work was supported by the Mishima Kaiun Memorial Foundation. The authors are very grateful to Tetsuya Tanigawa for his advice.

Author details
[1]Department of Plastic Surgery, Osaka University Graduate School of Medicine, Suita-shi, Osaka, Japan. [2]Department of Child Development and Molecular Brain Science, United Graduate School of Child Development, Osaka University, Suita-shi, Osaka, Japan. [3]Department of Research & Development Noevir Co., Ltd. Higashiomi, Shiga, Japan. [4]Division of Molecular Brain Science, Research Institute of Traditional Asian Medicine, Kinki University, Osakasayama, Osaka, Japan. [5]Division of Plastic and Reconstructive Surgery, Niigata University Graduate School of Medicine, Niigata-shi, Niigata, Japan.

Received: 24 September 2013 Accepted: 24 March 2014
Published: 8 April 2014

References

1. Baumann L: **Skin ageing and its treatment.** *J Pathol* 2007, **211**:241–251.
2. Fenske NA, Lober CW: **Structural and functional changes of normal aging skin.** *J Am Acad Dermatol* 1986, **15**:571–585.
3. Callaghan TM, Wilhelm KP: **A review of ageing and an examination of clinical methods in the assessment of ageing skin. Part I: Cellular and molecular perspectives of skin ageing.** *Int J Cosmet Sci* 2008, **30**:313–322.
4. Rice-Evans CA, Miller NJ, Paganga G: **Structure-antioxidant activity relationships of flavonoids and phenolic acids.** *Free Radic Biol Med* 1996, **20**:933–956.
5. Valcic S, Muders A, Jacobsen NE, Liebler DC, Timmermann BN: **Antioxidant chemistry of green tea catechins. Identification of products of the reaction of (–)-epigallocatechin gallate with peroxyl radicals.** *Chem Res Toxicol* 1999, **12**:382–386.
6. Ruch RJ, Cheng SJ, Klaunig JE: **Prevention of cytotoxicity and inhibition of intercellular communication by antioxidant catechins isolated from Chinese green tea.** *Carcinogenesis* 1989, **10**:1003–1008.
7. Higdon JV, Frei B: **Tea catechins and polyphenols: health effects, metabolism, and antioxidant functions.** *Crit Rev Food Sci Nutr* 2003, **43**:89–143.
8. Cavet ME, Harrington KL, Vollmer TR, Ward KW, Zhang JZ: **Anti-inflammatory and anti-oxidative effects of the green tea polyphenol epigallocatechin gallate in human corneal epithelial cells.** *Mol Vis* 2011, **17**:533–542.
9. Steinmann J, Buer J, Pietschmann T, Steinmann E: **Anti-infective properties of epigallocatechin-3-gallate (EGCG), a component of green tea.** *Br J Pharmacol* 2013, **168**:1059–1073.
10. Sharma A, Gupta S, Sarethy IP, Dang S, Gabrani R: **Green tea extract: possible mechanism and antibacterial activity on skin pathogens.** *Food Chem* 2012, **135**:672–675.
11. Achour M, Mousli M, Alhosin M, Ibrahim A, Peluso J, Muller CD, Schini-Kerth VB, Hamiche A, Dhe-Paganon S, Bronner C: **Epigallocatechin-3-gallate up-regulates tumor suppressor gene expression via a reactive oxygen species-dependent down-regulation of UHRF1.** *Biochem Biophys Res Commun* 2013, **430**:208–212.
12. Zhang Y, Yang ND, Zhou F, Shen T, Duan T, Zhou J, Shi Y, Zhu XQ, Shen HM: **(–)-Epigallocatechin-3-gallate induces non-apoptotic cell death in human cancer cells via ROS-mediated lysosomal membrane permeabilization.** *PLoS One* 2012, **7**:e46749.
13. Fujimura Y, Sumida M, Sugihara K, Tsukamoto S, Yamada K, Tachibana H: **Green tea polyphenol EGCG sensing motif on the 67-kDa laminin receptor.** *PLoS One* 2012, **7**:e37942.
14. Naderi J, Hung M, Pandey S: **Oxidative stress-induced apoptosis in dividing fibroblast involves activation of p38 MAP kinase and over-expression of Bax: resistance of quiescent cells to oxidative stress.** *Apoptosis* 2003, **8**:91–100.
15. Alster TS, West TB: **Human-derived and new synthetic injectable materials for soft-tissue augmentation: current status and role in cosmetic surgery.** *Plast Reconstr Surg* 2000, **105**:2515–2525.
16. Eça LP, Pinto DG, de Pinho AM, Mazzetti MP, Odo ME: **Autologous fibroblast culture in the repair of aging skin.** *Dermatol Surg* 2012, **38**:180–184.
17. Jäger C, Brenner C, Habicht J, Wallich R: **Bioactive reagents used in mesotherapy for skin rejuvenation *in vivo* induce diverse physiological processes in human skin fibroblasts *in vitro*- a pilot study.** *Exp Dermatol* 2012, **21**:72–75.
18. Solakoglu S, Tiryaki T, Ciloglu SE: **The effect of cultured autologous fibroblasts on longevity of cross-linked hyaluronic acid used as a filler.** *Aesthet Surg J* 2008, **28**:412–416.
19. Feng B, Fang Y, Wei SM: **Effect and mechanism of epigallocatechin-3-gallate (EGCG). against the hydrogen peroxide-induced oxidative damage in human dermal fibroblasts.** *J Cosmet Sci* 2013, **64**:35–44.
20. Liu J, Lin A: **Role of JNK activation in apoptosis: a double-edged sword.** *Cell Res* 2005, **15**:36–42.
21. Wada T, Penninger JM: **Mitogen-activated protein kinases in apoptosis regulation.** *Oncogene* 2004, **23**:2838–2849.
22. Yang CS, Wang X, Lu G, Picinich SC: **Cancer prevention by tea: animal studies, molecular mechanisms and human relevance.** *Nat Rev Cancer* 2009, **9**:429–439.
23. Liang YJ, Jian JH, Liu YC, Juang SJ, Shyu KG, Lai LP, Wang BW, Leu JG: **Advanced glycation end products-induced apoptosis attenuated by PPARδ activation and epigallocatechin gallate through NF-κB pathway in human embryonic kidney cells and human mesangial cells.** *Diabetes Metab Res Rev* 2010, **26**:406–416.
24. Choi YJ, Jeong YJ, Lee YJ, Kwon HM, Kang YH: **(–)Epigallocatechin gallate and quercetin enhance survival signaling in response to oxidant-induced human endothelial apoptosis.** *J Nutr* 2005, **135**:707–713.

doi:10.1186/1472-6882-14-133
Cite this article as: Tanigawa *et al.*: (+)-Catechin protects dermal fibroblasts against oxidative stress-induced apoptosis. *BMC Complementary and Alternative Medicine* 2014 **14**:133.

Journal of Cosmetic Dermatology, 13, 158–163

Objective assessment of facial skin aging and the associated environmental factors in Japanese monozygotic twins

Ryoko Ichibori, MD,[1] Takashi Fujiwara, MD,[1] Tomoko Tanigawa, MD,[1] Shigeyuki Kanazawa, MD, PhD,[1] Kenta Shingaki, PhD,[2] Kosuke Torii, PhD,[2] Koichi Tomita, MD, PhD,[1] Kenji Yano, MD, PhD,[1] Osaka Twin Research Group[3] Yasuo Sakai, MD, PhD,[1] & Ko Hosokawa, MD, PhD[1]

[1]*Department of Plastic Surgery, Osaka University Graduate School of Medicine, Osaka, Japan*
[2]*Department of Research & Development, Noevir Co. Ltd., Shiga, Japan*
[3]*Department of Osaka Twin Research Center, Osaka University, Osaka, Japan*

Summary

Twin studies, especially those involving monozygotic (MZ) twins, facilitate the analysis of factors affecting skin aging while controlling for age, gender, and genetic susceptibility. The purpose of this study was to objectively assess various features of facial skin and analyze the effects of environmental factors on these features in MZ twins. At the Osaka Twin Research Center, 67 pairs of MZ twins underwent medical interviews and photographic assessments, using the VISIA® Complexion Analysis System. First, the average scores of the right and left cheek skin spots, wrinkles, pores, texture, and erythema were calculated; the differences between the scores were then compared in each pair of twins. Next, using the results of medical interviews and VISIA data, we investigated the effects of environmental factors on skin aging. The data were analyzed using Pearson's correlation coefficient test and the Wilcoxon signed-rank test. The intrapair differences in facial texture scores significantly increased as the age of the twins increased ($P = 0.03$). Among the twin pairs who provided answers to the questions regarding history differences in medical interviews, the twins who smoked or did not use skin protection showed significantly higher facial texture or wrinkle scores compared with the twins not exposed to cigarettes or protectants ($P = 0.04$ and 0.03, respectively). The study demonstrated that skin aging among Japanese MZ twins, especially in terms of facial texture, was significantly influenced by environmental factors. In addition, smoking and skin protectant use were important environmental factors influencing skin aging.

Keywords: twin study, skin aging, environmental factors

Introduction

Many studies investigating the relationships between skin aging and environmental factors have been reported.[1–4] These studies have indicated that environmental factors, including ultraviolet irradiation and cigarette smoking, markedly influence skin aging. Other environmental factors, such as body mass index (BMI), alcohol consumption, and marital status have also been

Correspondence: R Ichibori, Department of Plastic Surgery, Osaka University Graduate School of Medicine, 2-2 C11 Yamadaoka, Suita-city, Osaka 565-0871 Japan. E-mail: ryoko.ichibori-20@live.jp

Accepted for publication November 27, 2013

suggested to be associated with skin aging.[2,5,6] Twin studies, especially those involving monozygotic (MZ) twins, provide unique opportunities to control for age, gender, and genetic effects in the analysis of the effects of environmental factors on skin aging.[5,7]

In the present study, we conducted medical interviews and facial photographic assessments of 67 pairs of adult, Japanese, MZ twins between 2010 and 2013. This study, conducted at the Osaka Twin Research Center, evaluated the influence of environmental factors on skin aging. Using a complexion analysis system, facial features were objectively evaluated. This was the first trial of its kind on a Japanese population.

Patients and methods

The subjects included 67 pairs of adult, MZ twins visiting the Osaka Twin Research Center. The Research Center was set up in 2010 at Osaka University, to provide comprehensive medical examinations to Japanese MZ and dizygotic adult twins. Volunteers for the twin study were recruited from the general community through various media advertisements. The study was approved by the Osaka University ethics committee, and all of the participants provided written, informed consent.

The MZ twins included 27 pairs of men and 40 pairs of women, aged 40–87 years. The subjects participated in medical interviews and photographic assessments designed to analyze the important visible features of facial skin aging. The medical interviews were conducted using a structured questionnaire to collect information regarding: age, alcohol consumption, smoking history, marital status, hormone replacement therapy, medical history, sun exposure history, BMI, and sunscreen or foundation use.

Photographic assessments were performed using the VISIA® Complexion Analysis System (Canfield Scientific., Fairfield, NJ, USA; Fig. 1).[8–10] The VISIA System, with a configurable head support, ensured consistent positioning of each subject's head. The subjects cleaned their skin with a gentle facial makeup remover before the image was obtained. The photographic images were captured with standard, cross-polarized, parallel polarized, and ultraviolet light. Images were taken in two different close-up views (right lateral 37°, left lateral 37°) for each subject to quantify the scores and percentiles of the cheek skin, including spots, wrinkles, pores, texture, and erythema. The percentiles enabled the evaluation of the subject's complexion analysis results through a comparison between the individual's scores and those of people of the same sex, generation, and skin type in the database. The scores provided a comprehensive measurement of the impact that each feature had on the client's complexion. The scores factored in the total size and area, as well as the intensity

Figure 1 Photographic images acquired by the VISIA® Complexion Analysis System. Two close-up views show spots and wrinkles over the subject's cheek.

of the feature being analyzed. Skin with a lower score for each factor was considered to be more youthful in appearance (values ranged from 0 to 100). In the present study, we used the scores to more objectively assess skin condition. Skin texture represents the degree of uniformity of the surface of cheek skin. A subject with shallow sulcus cutis and closely shaped crista cutis was considered to have tidy skin. Skin wrinkle indicated to folds resulting from dermal connective tissues including elastic and collagen fibers.

The average scores for the right and left cheeks were calculated, and the differences between individuals in each pair of twins were recorded and chronologically compared. In addition, the results of the pairs of twins who provided answers to the medical interviews were compared with the VISIA data to explore the effects of environmental factors on their facial features. The twin pairs who differed by more than 4 BMI points from each other were also compared.

All calculations were performed with the JMP statistical software package (SAS, Cary, NC, USA). The data were analyzed using Pearson's correlation coefficient test and the Wilcoxon signed-rank test; a *P*-value of <0.05 was considered statistically significant.

Results

Of the 67 pairs of MZ twins, two male pairs were excluded from the analysis due to the interference of their mustaches, with the photographic assessments. Therefore, 25 pairs of men and 40 pairs of women were evaluated in this study. The patients had a range of Fitzpatrick skin types, from II to IV.

Subject's baseline characteristics

The characteristics of the evaluated subjects, based on their medical interviews, are presented in Table 1. The subjects ranged in age from 40 to 87 years and represented all the regions in Japan. Alcohol consumption, smoking histories, and outdoor work were more frequent among men than women, although sunscreen or foundation use was more frequent in women. In 11 twin pairs, the individuals differed from each other by more than 4 BMI points.

VISIA® complexion analysis system assessments

By using the VISIA® system, differences in facial feature scores (facial spots, wrinkles, pores, texture, and erythema) in each pair of twins were calculated and chronologically compared, by comparing the results for twins of various ages. The results of the intrapair comparisons are shown in Fig. 2. As the ages of the twins increased, the intrapair differences in facial texture scores also increased ($P = 0.03$). However, significant correlations between increasing ages and intrapair differences in facial spots, wrinkles, pores, and erythema were not observed ($P = 0.27$, 0.08, 0.63, and 0.23, respectively).

Environmental factors

Alcohol consumption, smoking history, hormone replacement therapy, sun exposure history, sunscreen or foundation use, marital status, medical history, and BMI were also investigated for their effects on facial skin aging. Comparing the VISIA scores of each factor in the twins of each pair, the twins who smoked showed significantly higher facial texture scores compared with the twins who were nonsmokers ($P = 0.04$). The twins who did not use sunscreen or foundation also showed significantly higher facial wrinkle scores compared with the twins who used these products ($P = 0.03$) (Table 2). There were no significant intrapair differences in the other environmental factors, namely alcohol consumption, hormone replacement therapy, sun exposure history, marital status, medical history, or BMI.

Discussion

Skin aging is influenced by the interaction of both intrinsic and extrinsic factors.[11,12] Intrinsic aging is an inevitable process that is regulated by a genetically programmed pattern, characterized by cellular senescence, decreased proliferative capacity, decreased cellular DNA repair capacity, oxidative stress, and gene mutations. Extrinsic aging is regulated by various external factors such as ultraviolet irradiation, cigarette smoking, alcohol consumption, marital status, and medical history.[2,5,6,13] Skin aging is manifested as spots, wrinkles, pores, coarseness, and telangiectasia, which are significantly correlated with the appearance of elderly individuals.[14,15] Therefore, accurate assessment of facial features is of great importance for esthetic surgeries and may also provide important information about several skin disorders.

There have been many reports regarding the relationship between skin aging and environmental factors.[1–4,16] Up to 40% of the changes that contribute to an aged appearance are reported to be due to nongenetic factors.[2,15] The first proposed correlation between smoking and skin aging was made by Solly in 1856.[17]

Table 1 Baseline characteristics of subjects

	Men (n = 25) No. of twin pairs (%)	Women (n = 40) No. of twin pairs (%)
Age		
	0 (0.0)	7 (17.5)
40–49		
	3 (12.0)	6 (15.0)
50–59		
	4 (16.0)	18 (45.0)
60–69		
	8 (32.0)	7 (17.5)
70–79		
	10 (40.0)	2 (5.0)
80–89		
Alcohol consumption: Twin1/Twin2		
	16 (64.0)	13 (32.5)
(+)/(+)		
	4 (16.0)	8 (20.0)
(+)/(−)		
	5 (20.0)	19 (47.5)
(−)/(−)		
History of smoking		
	18 (72.0)	4 (10.0)
(+)/(+)		
	2 (8.0)	6 (15.0)
(+)/(−)		
	5 (20.0)	30 (75.0)
(−)/(−)		
Marital status		
	23 (92.0)	32 (80.0)
(+)/(+)		
	1 (4.0)	5 (12.5)
(+)/(−)		
	0 (0.0)	2 (5.0)
(−)/(−)		
	1 (4.0)	1 (2.5)
Missing		
Sun exposure		
Outdoor work		
	10 (40.0)	4 (10.0)
(+)/(+)		
	7 (28.0)	7 (17.5)
(+)/(−)		
	8 (32.0)	29 (72.5)
(−)/(−)		
Outdoor sports		
	7 (28.0)	12 (30.0)
(+)/(+)		
	8 (32.0)	11 (27.5)
(+)/(−)		
	10 (40.0)	17 (42.5)
(−)/(−)		
Sunscreen or foundation use		
(+)/(+)	0 (0.0)	30 (75.0)
	3 (12.0)	6 (15.0)
(+)/(−)		
	22 (88.0)	4 (10.0)
(−)/(−)		
Medical history		
Diabetes		
(+)/(+)	1 (4.0)	4 (10.0)
	4 (16.0)	2 (5.0)
(+)/(−)		
	20 (80.0)	34 (85.0)
(−)/(−)		
Cardiovascular disease		
(+)/(+)	0 (0.0)	1 (2.5)
	2 (8.0)	1 (2.5)
(+)/(−)		
	23 (92.0)	38 (95.0)
(−)/(−)		
Asthma		
(+)/(+)	0 (0.0)	1 (2.5)
	0 (0.0)	0 (0.0)
(+)/(−)		
	25 (100.0)	39 (97.5)
(−)/(−)		
Depression		
(+)/(+)	0 (0.0)	0 (0.0)
	0 (0.0)	2 (5.0)
(+)/(−)		
	25 (100.0)	38 (95.0)
(−)/(−)		
History of hormone replacement therapy		
(+)/(+)	0 (0.0)	2 (5.0)
	2 (8.0)	9 (22.5)
(+)/(−)		
	23 (92.0)	29 (72.5)
(−)/(−)		
	Mean (range)	Mean (range)
Body mass index	22.9 (14.9–30.8)	21.6 (17.1–27.8)

Sun exposure has also been associated with an older appearance and has been suggested to accelerate with age. Similarly, a history of outdoor activities and failure to use sunscreen has been correlated with an older appearance.[5,16] Guyuron *et al.*[6] reported that the use of hormone replacements helped to preserve a younger appearance. The use of antidepressants, various diseases (diabetes, asthma, and cardiovascular disease), marital status, alcohol consumption, and BMI have also been suggested to be associated with skin aging.[2,5,6] Despite the number of studies on skin aging, the effects of various environmental factors are still not conclusively understood.

The study of twins, especially MZ twins, provides a unique opportunity to control for age, gender, and genetic susceptibility to aging in order to analyze environmental influences on aging. Gunn *et al.* performed heritability analyses of skin aging features in the twin

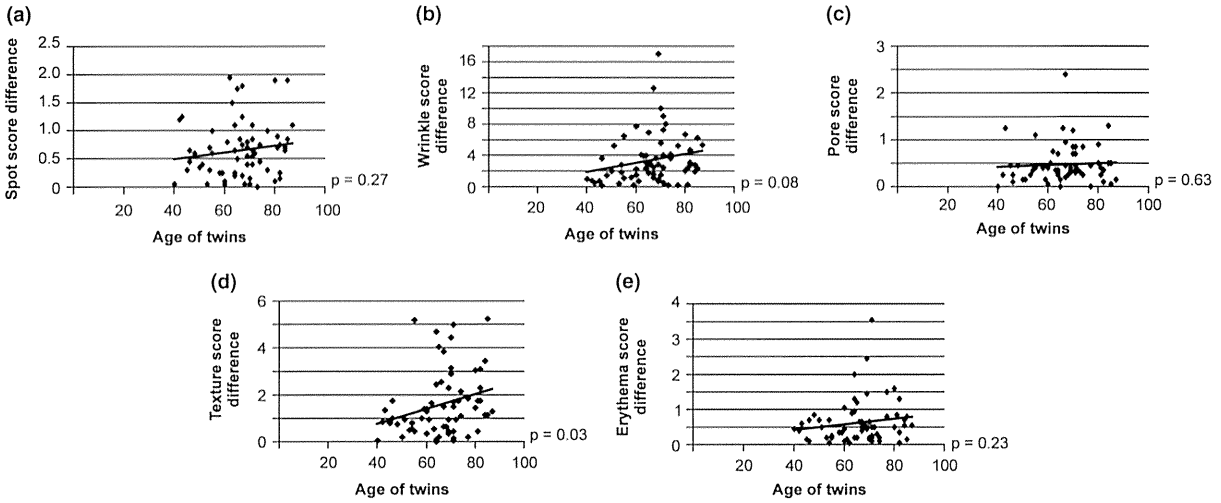

Figure 2 The differences in the VISIA scores for spots, wrinkles, pores, texture, and erythema in twin pairs. As the age of the twin increased, the intrapair differences in texture scores significantly increased as well ($P = 0.03$).

Table 2 Comparison of the VISIA scores of each factor in the twins of each pair who provided answers to the medical interviews

	Average VISIA score				
	Spots	Wrinkles	Pores	Texture	Erythema
Alcohol consumption (+) (n = 12)	3.63	8.94	2.25	4.33	3.73
Alcohol consumption (−) (n = 12)	3.56	8.76	2.06	3.86	3.4
Smoking (+) (n = 8)	3.85	13.39	2.88	6.11*	4.49
Smoking (−) (n = 8)	3.83	9.64	2.57	4.46*	3.89
Hormone replacement (+) (n = 11)	3.2	8.02	2.21	4.35	3.36
Hormone replacement (−) (n = 11)	3.21	8.06	2.19	4.15	3.48
Sun exposure (+) (n = 19)	3.48	8.91	2.02	3.48	3.62
Sun exposure (−) (n = 19)	3.88	8.8	2.11	4.11	3.74
Marital status (+)† (n = 6)	3.69	8.03	2.38	3.88	3.95
Marital status (−)† (n = 6)	3.46	8.43	2.53	4.89	3.74
Diabetes (+) (n = 6)	4.47	12.38	2.93	6.09	4.44
Diabetes (−) (n = 6)	4.16	10.74	3.02	5.87	4.29
Cardiovascular disease (+) (n = 3)	4.12	9.4	3.02	6.02	4.18
Cardiovascular disease (−) (n = 3)	4.27	12.7	2.75	5.88	4.35
Depression (+) (n = 2)	4.83	10.23	2.23	4.33	3.83
Depression (−) (n = 2)	4.02	11.63	1.83	3.88	3.98
Foundation or sunscreen use (+) (n = 9)	3.82	7.91*	2.27	4.26	3.56
Foundation or sunscreen use (−) (n = 9)	3.88	11.71*	2.35	4.62	3.73
Body mass index (large)‡ (n = 11)	3.76	11.47	3.05	6.35	4.13
Body mass index (small)‡ (n = 11)	4.08	13.6	2.82	5.95	4.26

The numbers are the average scores of each twin.
*<0.05
†Marital status (+) twin showed the twins who were married. Marital status (−) twin showed the twins who were not married.
‡The BMI (large) was >4 BMI points of the BMI (small).

population and demonstrated that 41–60% of the variations in sun damage, skin wrinkling, wrinkle depth, and pigmented age spot measurements were explained by genetic factors.[12] Shekar *et al.*[18] concatenated the variations in epidermal reticular patterning into genetic and environmental influences and estimated

the concomitant effects of sun exposure and skin color in MZ twins.

The objective evaluation of the characteristic features of the facial skin, however, has rarely been reported. The VISIA® Complexion Analysis System enables the procurement of high-quality digital facial photographs with standardized lighting and configurable head positioning. The images obtained allow the quantitation of the physical properties of the cheek skin, such as spots, wrinkles, pores, texture, and erythema. Differences in these properties between individual MZ twins were objectively analyzed, in this study, by the VISIA system.

The results indicated that as the age of the twins increased, the intrapair differences in facial texture scores also increased significantly ($P = 0.03$), suggesting that facial texture tends to be influenced by environmental factors. Environmental factors, including smoking and failure to use sunscreen or foundation, resulted in significantly higher facial texture and wrinkle scores ($P = 0.04$ and 0.03, respectively). These observations suggest that cigarette smoking and skin protection might markedly affect skin aging. Alcohol consumption, hormone replacement use, sun exposure history, marital status, medical history, and BMI did not demonstrate a significant correlation with facial skin aging. These results did not completely support previous reports, possibly due to the more objective assessments achieved using the VISIA system. However, ethnic differences may also affect skin aging.

The main limitation of this study was the sample size. If the sample sizes for most factors were sufficiently large, the intrapair differences of most environmental factors would be expected to be more significant. Moreover, our study had a bias toward a disproportionate number of female subjects. If more male subjects were included, the impact of additional environmental factors might be more apparent. Further investigations may help clarify the relationship between other environmental factors and skin aging in MZ twins.

As the age of the twins increased, facial texture scores were less similar between individual twins, within a pair. This suggests that facial texture is influenced by environmental factors rather than solely by genetic factors. Moreover, smoking and the failure to use skin protection resulted in significantly higher facial texture and wrinkle scores. These environmental factors were identified as important environmental factors contributing to skin aging.

References

1 Asakura K, Nishiwaki Y, Milojevic A *et al.* Lifestyle factors and visible skin aging in a population of Japanese elders. *J Epidemiol* 2009; **19**: 251–259.

2 Rexbye H, Petersen I, Johansens M *et al.* Influence of environmental factors on facial ageing. *Age Ageing* 2006; **35**: 110–115.

3 Diffey BL. The impact of topical photoprotectants intended for daily use on lifetime ultraviolet exposure. *J Cosmet Dermatol* 2011; **10**: 245–250.

4 Mayes AE, Murray PG, Gunn DA *et al.* Environmental and lifestyle factors associated with perceived facial age in Chinese women. *PLoS ONE* 2010; **5**: e15270.

5 Martires KJ, Fu P, Polster AM *et al.* Factors that affect skin aging. *Arch Dermatol* 2009; **145**: 1375–1379.

6 Guyuron B, Rowe DJ, Weinfield AB *et al.* Factors contributing to the facial aging of identical twins. *Plast Reconstr Surg* 2009; **123**: 1321–1331.

7 Doshi DN, Hanneman KK, Cooper KD. Smoking and skin aging in identical twins. *Arch Dermatol* 2007; **143**: 1543–1546.

8 Herane MI, Orlandi C, Zegpi E *et al.* Clinical efficacy of adapalene (differin (®)) 0.3% gel in Chilean women with cutaneous photoaging. *J Dermatolog Treat* 2012; **23**: 57–64.

9 Chan NP, Shek SY, Yu CS *et al.* Safety study of transcutaneous focused ultrasound for non-invasive skin tightening in Asians. *Lasers Surg Med* 2011; **43**: 366–375.

10 Seadi N, Petrell K, Arndt K *et al.* Evaluating facial pores and skin texture after low-energy nonablative fractional 1440-nm laser treatments. *J Am Acad Dermatol* 2013; **68**: 113–118.

11 Uitto J. The role of elastin and collagen in cutaneous aging: intrinsic aging versus photoexposure. *J Drugs Dermatol* 2008; **7**: s12–s16.

12 Larnier C, Ortonne JP, Venot A *et al.* Evaluation of cutaneous photodamage using a photographic scale. *Br J Dermatol* 1994; **130**: 167–173.

13 Chung JH, Lee SH, Youn CS *et al.* Cutaneous photodamage in Koreans. *Arch Dermatol* 2001; **137**: 1043–1051.

14 Gunn DA, Rexbye H, Griffiths CE *et al.* Why some women look young for their age. *PLoS ONE* 2009; **4**: e8021.

15 Christensen K, Iachina M, Rexbye H *et al.* "Looking old for your age": genetics and mortality. *Epidemiology* 2004; **15**: 251–252.

16 Kennedy C, Bastiaens MT, Bajdik CD *et al.* Effect of smoking and sun on the aging skin. *J Invest Dermatol* 2003; **120**: 548–554.

17 Solly S. Clinical lectures on paralysis. *Lancet* 1856; **2**: 641–643.

18 Shekar SN, Luciano M, Duffy DL *et al.* Genetic and environmental influences on skin pattern deterioration. *J Invest Dermatol* 2005; **125**: 1119–1129.

Hernia (2014) 18:587–590
DOI 10.1007/s10029-013-1152-1

CASE REPORT

Repair of symptomatic perineal hernia with a titanium mesh

Y. Imagawa · K. Tomita · K. Kitahara · K. Yano · K. Hosokawa

Received: 15 March 2013 / Accepted: 28 July 2013 / Published online: 10 August 2013

Abstract
Purpose Surgical repair of symptomatic perineal hernia is challenging, especially via a perineal approach with limited exposure of the hernia sac. Furthermore, insecure fixation of autologous or synthetic materials to bony structures often results in recurrence. Here, we describe the application of a titanium mesh for perineal hernia repair.
Methods We performed hernia repair with a thin titanium mesh via a perineal approach in three patients who developed secondary perineal hernia following abdominoperineal resection. After the hernia sac was isolated and dissected, the titanium mesh was molded and placed over the ischium and coccyx to support the pelvic floor.
Results No major complications occurred, and all three patients were free of recurrence at follow-up after 73, 109, and 6 months, respectively. The patients experienced slight pain in the perineal region when sitting, which resolved within 6 months.
Conclusion Our successful preliminary results indicate that a titanium mesh is useful for perineal hernia repair by the perineal approach, as it can provide rigid support for the pelvic floor by its entire surface while ensuring stability without any fixation.

Keywords Perineal hernia · Titanium mesh · Perineal approach · Abdominoperineal resection

Y. Imagawa · K. Tomita (✉) · K. Kitahara · K. Yano · K. Hosokawa
Department of Plastic and Reconstructive Surgery, Graduate School of Medicine, Osaka University, 2-2 C11 Yamadaoka, Suita-shi, Osaka 565-0871, Japan
e-mail: ktomita9@hotmail.co.jp

Introduction

Symptomatic perineal hernia is a relatively rare complication following major pelvic surgery. Secondary perineal hernia after abdominoperineal resection was first reported by Yeoman in 1939 [1]. This complication occurs usually within 1 year postoperatively, with reported incidence rates of approximately 1 and 10 % following abdominoperineal resection and pelvic exenteration, respectively [2–4]. Surgery is the only effective treatment for perineal hernia, although the complex anatomy of the pelvic floor and high abdominal pressure make the management challenging. To date, a number of surgical techniques have been reported, including simple closure of the pelvic defect and use of autologous and prosthetic materials such as fascia lata grafts and polypropylene meshes; however, a "gold standard" of care has yet to be established [3, 5–7].

Here, we present three cases of symptomatic perineal hernia repair performed via a perineal approach with a thin titanium mesh, which provides rigid support for the pelvic floor, while ensuring stability of bony structures without any fixation.

Case reports

Case 1

A 68-year-old female visited our hospital with painful bulging of the perineum (Fig. 1A) 13 months after she had undergone abdominoperineal resection (APR) for rectal cancer. A computed tomography (CT) scan showed a herniation of the small bowel protruding into the perineal area, confirming the diagnosis of a perineal hernia

(Fig. 1B). After cancer recurrence was excluded, a hernioplasty was performed in the jack-knife position via a perineal approach. A hernia sac was identified and the dissection proceeded in all directions until the bony structures were identified on each side and posterior aspect of the pelvic outlet. A titanium mesh (Titanium Micromesh MINI 2.0, Unimedic, Osaka, Japan), which was molded to measure approximately 2 cm longer in width than the patients' inter-ischiatic distance (measuring 14 × 10 cm, Fig. 1C), was inserted into the intra-peritoneal space and placed over the bilateral ischial tuberosities and coccyx. The mesh was stabilized without any fixation (Fig. 1D). To prevent direct contact between the mesh and small bowel, the surrounding adipose tissue was adequately interposed between the mesh and repaired hernia sac. No major postoperative complication was noted. The patient experienced slight pain in the perineal region when sitting, which resolved within 6 months. Regular follow-up with CT scan revealed no evidence of hernia recurrence or mesh malposition for more than 6 years (Fig. 2A–C).

Case 2 and 3

A 75-year-old female (case 2) and a 77-year-old female (case 3) visited our hospital with bulging of the perineum 9 and 12 months after they had undergone APR for rectal cancer, respectively. Indications for hernia repair were nausea caused by psychological stress due to bulging in the perineum in case 2, and a pain in the perineum in case 3. After cancer recurrence was excluded, a hernioplasty was performed via a perineal approach in the same manner as in case 1. Postoperative courses were uneventful in both cases, and there is no evidence of hernia recurrence for more than 9 years in case 2, and for 6 months in case 3.

The characteristics of the three patients are summarized in Table 1.

Discussion

There are three major approaches to perineal hernia repair: abdominal, perineal, and combined abdominoperineal

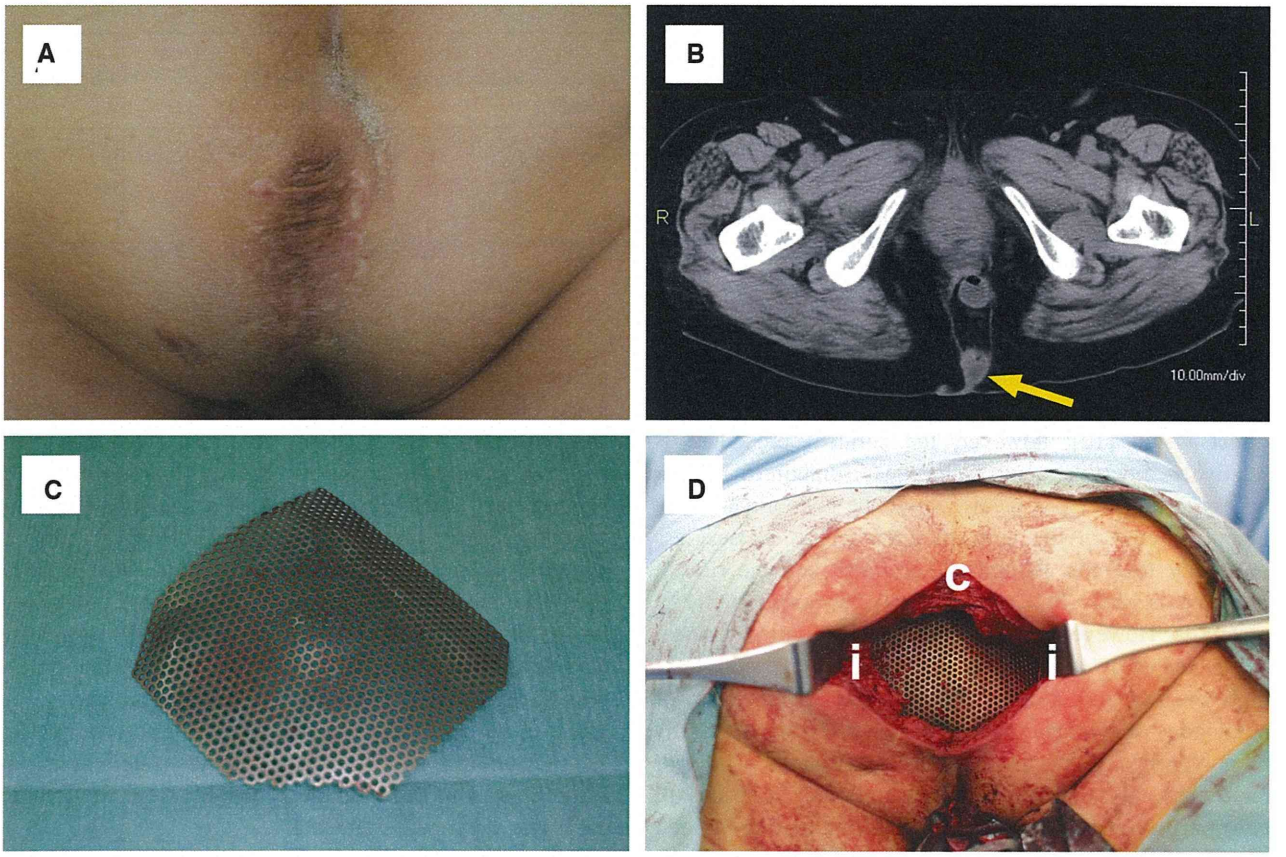

Fig. 1 **A** Preoperative image ("Case 1"). The patient suffered painful bulging in the perineal region. **B** Preoperative computed tomography scan revealed a herniation of the small bowel protruding into the perineum (*arrow*). Reproduced from Ref. [18] with permission. **C** A thin titanium mesh was molded intraoperatively to measure approximately 2 cm longer in width than the patient's inter-ischiatic distance. **D** The mesh was inserted into the intra-peritoneal space and placed over the bilateral ischial tuberosities (i) and coccyx (c). It gained stability without any fixation. Reproduced from Ref. [18] with permission

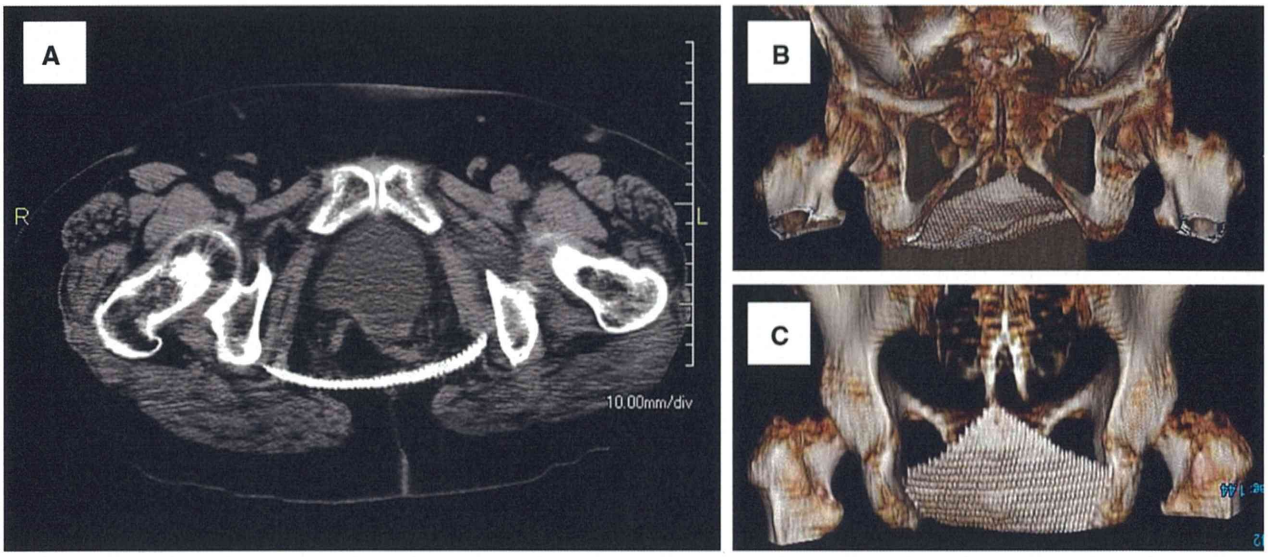

Fig. 2 **A** Computed tomography (CT) scan performed in "Case 1" 2 years post-hernioplasty revealed no hernia recurrence. Reproduced from Ref. [18] with permission. **B**, **C** Three-dimensional CT images obtained 2 years postoperatively show no malposition of the titanium mesh. Anterior view (**B**) and posterior view (**C**)

Table 1 Patient characteristics

Case no.	Age	Sex	Indication for repair	Type of initial operation	Period between initial operation and herniation (months)	Follow-up period (months)	Recurrence	Complications of hernioplasty
1	68	Female	Painful perineal bulging	APR	13	73	No	No
2	75	Female	Perineal bulging, nausea	APR	9	109	No	No
3	77	Female	Painful perineal bulging	APR	12	6	No	No

APR abdominoperineal resection

approaches [8, 9]. The abdominal approach allows mobilization of adherent bowel loops and fixation of autologous or synthetic materials to the bony pelvis under direct vision [10]; however, the surgical procedure is relatively invasive, and adhesions sometimes hinder access to the pelvic contents. Since the abdominal cavity is not entered in the perineal approach, it causes less morbidity than the abdominal approach, and the risk of infection is likely lower especially when using synthetic materials. However, the rate of recurrence after perineal hernia repair by the perineal approach is reportedly very high, ranging from 23 to 100 % [10–12]. Although use of autologous or synthetic materials such as fascia lata grafts or polypropylene meshes is a suitable option to prevent recurrence, adequate fixation of supportive materials to bony structures often present difficulties due to limited exposure. Furthermore, even if adequate fixation to the periosteum of the pelvis is achieved, the supportive materials without direct fixation to the bone can be gradually malpositioned due to the high shear stress between the periosteum and bone [13].

In our patients, we used a thin titanium mesh to support the pelvic floor. This material has been widely used in the field of maxillofacial surgery as it causes less foreign-body and hypersensitivity reactions [14, 15]. Importantly, the titanium mesh, which was molded to comfortably fit the pelvic defect, was securely placed over the bony structures via the perineal approach without requiring any fixation. In addition, unlike other synthetic materials such as polypropylene meshes, titanium mesh can provide rigid support for the pelvic floor by its entire surface, thereby decreasing the shear stress between the mesh and bony structures. A previous report suggested the risk of intestinal perforation due to adhesion of the synthetic mesh to the bowels [16]. To prevent this, we interposed an adequate volume of adipose tissue to avoid direct contact between the titanium mesh and repaired hernia sac.

Apart from adequate fixation, the strength of the support material is also a critical factor that can help prevent recurrence. Ego-Aguirre et al. [17] reported that, after repair of a perineal hernia following pelvic exenteration using a stainless steel wire mesh (Tantalum mesh), a late